

# Importance of Model Simulations in Cassini In-flight Mission Events

Jay Brown<sup>1</sup> and Eric Wang<sup>2</sup>

*Jet Propulsion Laboratory, California Institute of Technology, Pasadena, California, 91109*

Juan Hernandez<sup>3</sup> and Allan Y. Lee<sup>4</sup>

*Jet Propulsion Laboratory, California Institute of Technology, Pasadena, California, 91109*

Simulation environments have been an integral part of Cassini's heritage. From the time of flight software development and testing to the beginning of the spacecraft's extended mission operations, both softsim and hardware-in-the-loop testbeds have played vital roles in verifying and validating key mission events. Satellite flybys and mission-critical events have established the need to model Titan's atmospheric torque, Enceladus' plume density, and other key parametric spacecraft environments. This paper will focus on enhancements to Cassini's Flight Software Development System (FSDS) and Integrated Test Laboratory (ITL) to model key event attributes which establish valid test environments and ensure safe spacecraft operability. Comparisons between simulated to in-flight data are presented which substantiate model validity.

## Acronyms

<i>AACS</i>	= Attitude and Articulation Control Subsystem
<i>AFC</i>	= AACS Flight Computer
<i>CDS</i>	= Command and Data Subsystem
<i>DARTS</i>	= Dynamic Algorithms for Real Time Simulation
<i>FSDS</i>	= Flight Software Development System
<i>FSTB</i>	= Flight Software Test Bed
<i>FSW</i>	= Flight Software
<i>G&amp;C</i>	= Guidance and Control
<i>IEU</i>	= Image Emulation Unit
<i>INMS</i>	= Ion and Neutron Mass Spectrometer
<i>ITL</i>	= Integrated Test Laboratory
<i>ME</i>	= Main Engine
<i>RCS</i>	= Reaction Control System
<i>RWA</i>	= Reaction Wheel Assembly
<i>S/C</i>	= Spacecraft
<i>Tcl</i>	= Tool Command Language

## I. Introduction

ONE of the keys to the success of the Cassini mission is the ability to expose its software and hardware to realistic environments. Early in Cassini's infancy, scientific and engineering goals were defined which established spacecraft design and test needs. This identified the need to have capable test platforms which would

---

<sup>1</sup>Sr. Software Engineer, AACS FSW Cognizant Engineer, Guidance & Control Software and Flight Software Testing Group, 4800 Oak Grove Drive, M/S 230-104, Member AIAA. E-mail: jay.brown@jpl.nasa.gov.

<sup>2</sup>Assoc. Software Engineer, AACS FSW Engineer, Guidance & Control Software and Flight Software Testing Group, 4800 Oak Grove Drive, M/S 230-104.

<sup>3</sup>AACS Test Analyst, Integration and Testing Engineering Group, 4800 Oak Grove Drive, M/S 230-104.

<sup>4</sup>Project Element Manager, AACS, Cassini Spacecraft Operations Office, 4800 Oak Grove Drive, M/S 230-104.

expose software to mission-specific scenario environments. Examples would be sequence testing i.e. launch, main engine burns, etc., and fault scenario testing.

The capability of having a test environment that allowed quick and accurate verification of flight software was realized in early 1993 and its initial capabilities were released in late 1994 as the Flight Software Development System (FSDS). This was a faster-than-real-time softsim testbed which could be run on the same development workstations used to code the flight software. FSDS provided an environment to closely emulate the attitude control subsystem which interfaced with the AACS flight software. The testbed became the workhorse to test flight software functionality.<sup>1</sup> Several papers have been written which have identified FSDS capabilities and usefulness.<sup>2,7,23,24</sup> The testbed was heavily utilized both pre and post launch by the flight software team. Its proven high fidelity during development made it a vital test platform during operations by the flight software and uplink teams. As Cassini performed its prime mission, it was evident that FSDS would have to simulate additional environments that Cassini would encounter in flight.

This paper will focus on mission scenarios which occurred during the Saturnian orbit. Key efforts were made to develop models to emulate the Titan atmosphere and Enceladus plume density which provided key capabilities to test the flight software in nominal and off-nominal environmental conditions. At the time, these models were validated using the best known methods to represent external environments. As in-flight data became available, the models were re-validated against actual environment data.

## II. Cassini Mission Overview

The Cassini-Huygens mission started in 1989 as part of NASA's Mariner Mark II program<sup>3</sup> which was initiated in 1987. In 1992, the mission and spacecraft were both redesigned which resulted in a simplified implementation of original scientific goals and engineering capabilities.

Cassini-Huygens, depicted in Figure 1, launched on a Titan IV-B/Centaur in the early morning of 15 October 1997 from Cape Canaveral. This was the beginning of its interplanetary in-flight operations to the sixth planet in the solar system – Saturn. While previous missions were flybys, Cassini is the first to orbit the planet. Cassini flew a Venus-Venus-Earth-Jupiter gravity assist trajectory to boost its velocity to reach Saturn in 6.7 years.

The prime tour would begin after a successful Saturn Orbit Insertion (SOI) on 30 June 2004. Six months later, Cassini successfully ejected the Huygens probe on 24 December 2004, where it finally reached its destination to Saturn's largest moon Titan on 14 January 2005, and transmitted three hours and forty minutes<sup>4</sup> of scientific data to Cassini. Cassini then embarked on a seventy-four orbit Saturnian prime mission. Throughout Cassini's four year prime mission, it has had forty-four encounters with Titan as well as three flybys of Enceladus.

The discovery of water expulsion from the southern surface region of Enceladus prompted a redesign of the extend mission which was approved in April 2008. Another twenty-seven Titan flybys and seven Enceladus flyby encounters are slated for a two year extension to September 2010.

## III. FSDS Overview and Capabilities

A key aspect of the FSDS environment is that AACS flight software was required to be in the loop, this process is illustrated in Figure 2. This provided flight software developers the fidelity needed to test in a pseudo-realistic environment that was comparable to the actual spacecraft environment with respect to AACS concerns. Flight software must synchronize and rely on to the simulator, and duration of activities must be modeled correctly. FSDS communicates via shared memory and signals with flight software. There is one UNIX process for each flight software processor, one process for the bulk of the simulation, and one process for the star tracker simulation, which

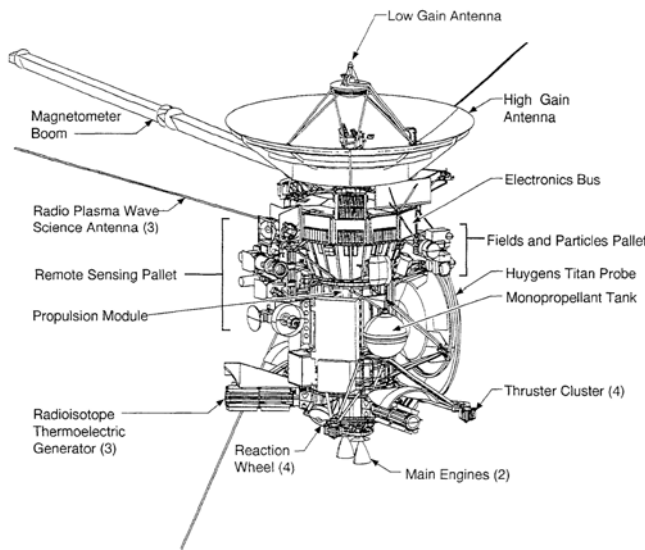


**Figure 1. Cassini Spacecraft.** *Cassini is the third heaviest (5,574 kilograms or 6 tons) spacecraft to ever be launched.*

run on a Sun Solaris/UNIX desktop workstation environment. FSDS uses a Tcl front-end allowing for adaptable user interface.

AACS architecture is a redundant subsystem with dual redundant data buses and dual AACS Flight Computers (AFCs) that can run prime and backup flight software simultaneously. FSDS had to accurately model the redundant architecture, as illustrated in Figure 3, to provide the fidelity needed to support credible flight software and scenario testing. Millisecond and microsecond level hardware behavior was simulated to create a virtual real-time execution environment. This keeps the correlation of events that happen in real-time, but executes faster due to the host workstation processor. The order of events would execute the same as a corresponding real-time testbed. This feature is vital to the realism of actual spacecraft performance. Detailed capabilities were captured in another paper,<sup>2</sup> so highlights are given below:

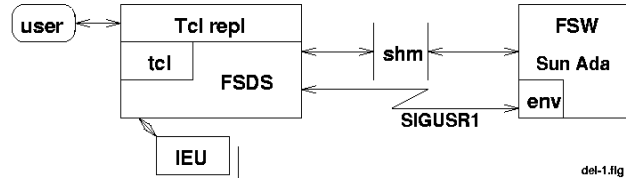


**Figure 2. FSDS, FSW, and IEU Processes Interface Environment (From Reference 2).** *The runtime environment used to model FSDS on a Sun Solaris platform.*

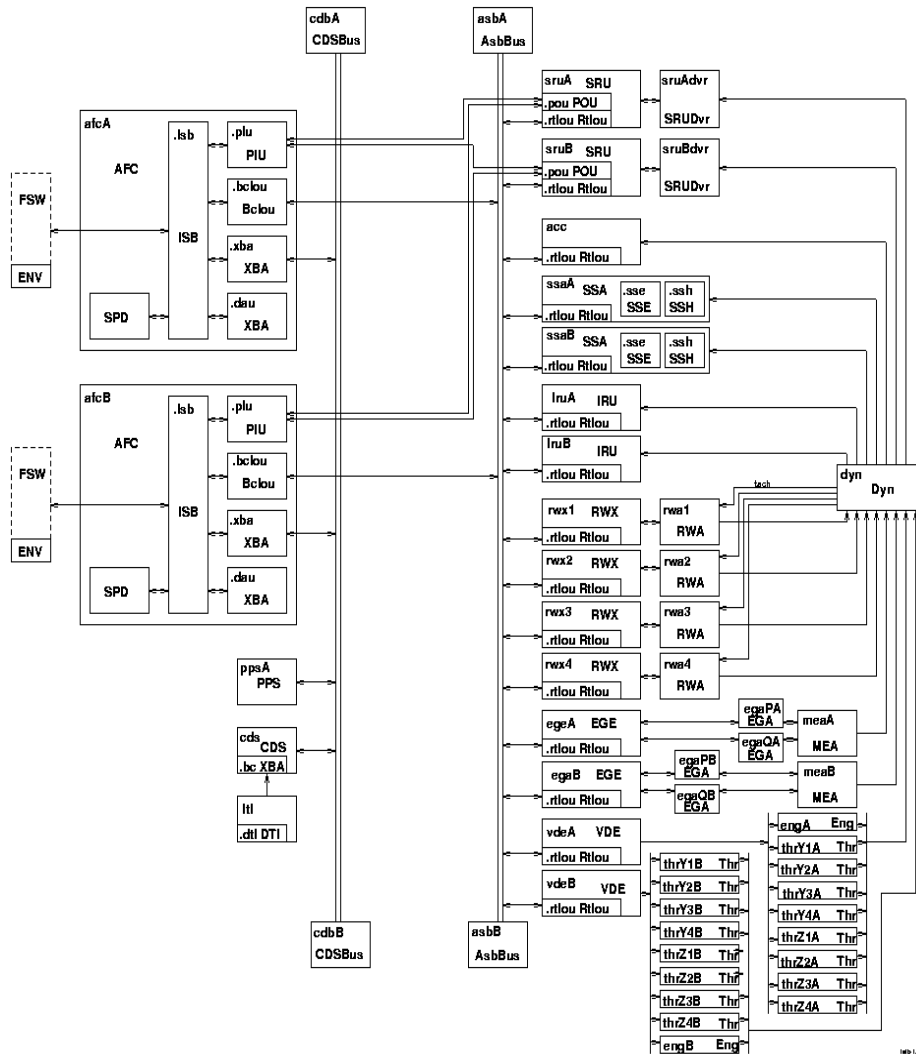


**Figure 3. Detailed FSDS Object Model Diagram (From Reference 2).** *Architecture focuses on actual hardware configuration. This represents the type and level of model detail that needs to be implemented in a softsim environment to provide the capability of predicting and reconstructing events at a fidelity that warrants accuracy, believability, and credibility.*

#### **A. FSDS contains high-fidelity models and services**

- 1) The dynamics engine used was DARTS,<sup>5</sup> which could accurately model multiple flexible bodies. The same dynamics models are used, but allow multiple S/C configurations (derived from structured finite element models), mass depletions, and user-programmed external forces and torques.
- 2) Redundant backplane, AACS, and Command and Data Subsystem (CDS) bus models are simulated to the register and packet level. This gives the ability to trace bus traffic and the ability to dump memory locations.
- 3) Models accurately emulate AACS actuators, sensors, and power and propulsion subsystems.
- 4) Emulated CDS functionality can simulate command and telemetry streams, watchdog timer, sending and receiving requests, recovery data, and state table data.
- 5) Fault injection capability could accurately model failure modes.

#### **B. Key FSDS capabilities**

- 1) A Tcl command engine allows users to interactively or through scripts retrieve and set parameters and variables in the hardware (physics) models, and peek and poke global variables in flight software. The Tcl interface allows interactive commanding to be sent, and telemetry streams to be observed and validated.
- 2) Ability to set initial time and clock time.
- 3) Use of ephemeris and S/C trajectory files to model precise S/C locations.
- 4) Can select multiple sets of S/C mass properties to simulate different phases of the Cassini mission.

These capabilities provide a framework that makes it easy to customize environments to suit the tester's needs. This made FSDS the primary testbed to run the majority of G&C and Fault Protection test scenarios varying and validating parameters for algorithm and control verification.<sup>6,7</sup>

Since FSDS is not real hardware model dependent, it runs as fast as the host CPU. Currently, a Sun Blade UNIX workstation can run the AACS Flight Software and FSDS at 5 to 6 times faster than real-time. Due to the faster than real-time capability, some disadvantages can occur which could mask out timing issues. The FSDS testbed cannot simulate a flight computer reset and recovery or a CDS to AACS communication loss, which can affect fault protection testing.<sup>2</sup>

### **IV. The Role of FSDS in Mission Operations**

FSDS transitioned from being only a FSW development testbed used for the verification and validation of FSW to a key ground software testbed used to validate spacecraft in-flight scenarios. Being able to simulate the environments or effects of what the FSW and spacecraft would encounter is an important capability that was and still is valuable to the flight operations team. Therefore, continual updates to FSDS have always remained a high priority to the operations team. During the operations phase of the Cassini mission, key limitations of FSDS were addressed. While not compromising the existing model verification and validation efforts during its core development cycle, new models and Tcl script wrappers were added to provide missing capabilities.

#### **A. Superscript**

Superscript was developed several years before Saturn Orbit Insertion to address FSDS critical sequence testing; allowing mark and rollback capabilities and a CDS System Fault Protection interface to AACS FSW. This was a vital addition which enabled the capability to test thousands of fault scenario test cases without having to rely on the time-limited and resource-limited hardware-in-the-loop testbeds. A key superscript enhancement addressed the simulation of a flight computer reset and recovery actions issued by or in response to CDS. While this capability mimicked the necessary communication interface messages and responses with CDS, the simulation of a hardware reset to the AFC computer and its associated timings were still an issue. The softsim could not mimic the physical disconnection and halt the software processes which would occur when a "real" flight computer went offline. FSW Fault Protection responses were still being issued when the AFC was intended to be in ROM or offline. For those special cases, the hardware-in-the-loop testbeds were utilized to capture the correct (lack of) FP commanding and timing during startup ROM initialization or before the AFC would come back online.

#### **B. Anticipating Future Mission Scenarios**

While the initial intent and design of FSDS focused on subsystem testing, its role to support scenario or sequence validation became just as important post launch. Such activities were addressing continual updates to key parameters that were phase dependent or a result of in-flight experience.

- 1) Changing ephemerides to support orbit scenarios.

- 2) Spacecraft mass properties updates – fuel depletion model, post Huygens probe ejection configuration, etc.
- 3) RCS and ME thruster force magnitudes, rise & fall time constants, etc.
- 4) Modeling of RWA friction spikes and drag torque.
- 5) Modeling misalignments of Stellar Reference Unit assemblies.
- 6) Threshold updates to Sun Sensor Assemblies.
- 7) Updates to new commands and telemetry to support critical sequences such as SOI and Probe Relay.

One of Cassini’s main science target objectives was Saturn’s moon Titan. Therefore, several years before Cassini’s first scheduled low-altitude Titan flyby, an effort was made to implement an atmospheric model to simulate the torque the spacecraft would experience when passing through its atmosphere.

To support Cassini’s planned and initial Enceladus flyby through its water plumes near the southern pole, another enhancement to FSDS would add a plume density model. The Enceladus plume density model is based on the Titan atmospheric model with modifications to density formulas and entry/exit criteria.

The remaining sections of this paper are dedicated to describing the efforts accomplished to implement both Titan and Enceladus models in support of ensuring safe flybys through nominal and fault scenarios testing.

## V. Titan Model Development and Validation

Titan is Saturn's largest moon. It is the second largest moon in the Solar System. Only Jupiter's moon Ganymede is larger. At 5150 kilometers in diameter, Titan is larger than either of the planets Mercury or Pluto. Titan orbits Saturn at a distance of 1,222,000 kilometers, taking 15.9 days to complete one revolution. Titan is of great interest to scientists because it is the only known moon in the Solar System with a “major” atmosphere. Titan's atmosphere is 10 times thicker than Earth's. Except for some clouds, Earth's surface is visible from space. But on Titan, a thick haze extending up to 200 kilometers above the surface obscures the entire surface from optical observations. Through ongoing observations from Earth as well as data collected by the Pioneer and Voyager spacecraft, scientists now know that Titan's atmosphere is composed primarily of nitrogen. One of the major science objectives of the Cassini mission is the characterization of Titan’s atmosphere constituent abundance. This science objective is to be achieved via 21, 18, and 26 low-altitude Titan flybys in the Prime, Extended, and Extended-extended Cassini missions, respectively. Table 1 summarizes the altitudes and latitudes of all the low-altitude Titan flybys that were executed in the Prime mission.

**Table 1. Low-altitude Titan Flybys in the Cassini Prime Mission.**

<b>Titan Flyby</b>	<b>Altitude at Closest Approach [km]</b>	<b>Latitude at Closest Approach [°]</b>	<b>Year Day-of-Year</b>
16	950	+85	2006-203
17	1000	+23	2006-250
18	960	+71	2006-266
19	980	+61	2006-282
20	1030	+8	2006-298
21	1000	+44	2006-346
23	1000	+31	2007-013
25	1000	+31	2007-053
26	980	+32	2007-069
27	1010	+41	2007-085
28	990	+51	2007-100
29	980	+59	2007-116
30	960	+69	2007-132
32	950	+84	2007-164
36	975	-60	2007-275
37	1000	-22	2007-323
39	970	-70	2007-354
40	1010	-12	2008-005
41	1000	-34	2008-053
42	1000	-27	2008-085
43	1000	+17	2008-133

### A. Titan Atmospheric Density Model

Cassini is controlled by thrusters during low-altitude Titan flybys. Thrusters are fired to overcome the atmospheric torque imparted on the spacecraft due to the Titan atmosphere as well as to slew the spacecraft in inertial space to meet the pointing needs of science instruments such as the Ion and Neutral Mass Spectrometer (INMS). The adequacy of the thrusters in providing control torque about all three spacecraft axes during a low-altitude Titan should not be taken for granted. To confirm the adequacy of the control authority of the Cassini control system, there is a need to accurately model the atmospheric torque imparted on the spacecraft:

$$\bar{T}_{\text{ATMO}}(t) \approx \frac{1}{2} C_D \rho_{\text{Titan}}(t) V(t)^2 A_{\text{Projected}}(t) \bar{u}_v(t) \times [\bar{r}_{\text{CP}}(t) - \bar{r}_{\text{CM}}] \quad (1)$$

In this equation,  $\rho_{\text{Titan}}$  is the Titan atmospheric density in  $\text{kg/m}^3$ . During a Titan flyby, the altitude of the spacecraft relative to the Titan surface first decreased and then increased with time. Since Titan atmospheric density is a strong function of the Titan-relative altitude,  $\rho_{\text{Titan}}$  is a time-varying quantity. The simulation testbed must provide a model that provides the atmosphere density as a function of altitude. A suitable model that has been adopted for this purpose is described in Reference 8 (see also Reference 9):

$$\rho_{\text{Titan}}(z, n) = 6.35 \times 10^{-3} \exp\left[-\frac{11400(z-76)}{T(z+2575)}\right] + 5.13 \times 10^{-4} \exp\left[-\frac{8030(z+429)}{T(z+2575)}\right] + 7.35 \times 10^{-2} \exp\left[-\frac{15000(z-44)}{T(z+2575)}\right] \quad (2)$$

In this expression,  $z$  (in km) is the Titan-relative altitude of the spacecraft. The first, second, and third terms in this expression represent the density “contributions” of nitrogen, methane, and Argon, respectively.  $T$  (K) is the atmosphere temperature and is given by  $T = 175 + 10n$ . A large “ $n$ ” value produces high atmosphere temperature and high density. This factor “ $n$ ” is used to tune the Titan atmosphere density model so that the resultant density matches flight result as close as possible. For an assumed value of  $n = 1$ , the variation of density with Titan-relative altitude is depicted in Figure 4.

The spacecraft velocity relative to Titan is denoted by  $V(t)$  (in m/s). Typically, the magnitude of  $V$  is on the order of 6 km/s. The orientation of this velocity vector as expressed in the S/C’s coordinate frame is denoted by the

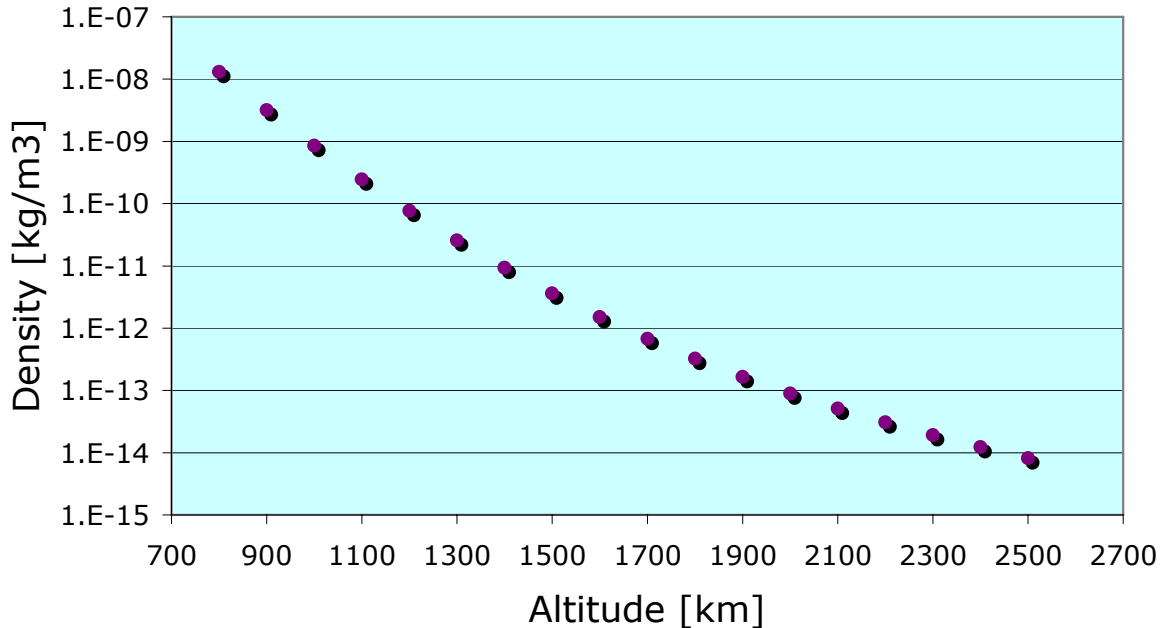


**Figure 4. Titan Density vs. Altitude.** Variation of Titan atmosphere density with Titan-relative altitude (in a semi-log plot).

unit vector  $u_V$ . The area of the spacecraft projected onto a plane that is perpendicular to the vector  $u_V$  is denoted by  $A_{\text{Projected}}$  (in  $m^2$ ). Since the spacecraft might be slewed during the flyby to achieve science objectives, the projected area will change continuously with time. The variation of the projected area with respect to the changing azimuth and elevation angles (between  $u_V$  and the spacecraft's body frame) is given in the simulation testbed. One convenient way to do this is to use a two-dimensional look-up table. The displacement vectors, from the origin of the spacecraft coordinate frame to the spacecraft's center of mass and center of pressure (in m) are denoted by  $r_{\text{CM}}$  and  $r_{\text{CP}}$ , respectively. Note that  $r_{\text{CM}}$  is a constant vector while the  $r_{\text{CP}}$  is a time-varying vector. Another look-up table is used to provide value of  $r_{\text{CP}}$  with respect to the azimuth and elevation angles. Finally, the dimensionless quantity  $C_D$  is the drag coefficient associated with the free molecular flow of Titan atmospheric constituents passed the body of the Cassini spacecraft. The drag coefficient  $C_D$  can be estimated using formulae given in References 10-12. In our work, we use  $C_D = 2.2$ .

Other non-gravitational torque imparted on the spacecraft during a low-altitude Titan flyby includes gravity gradient torque and magnetic torque. They are both small when compared with the atmospheric torque but are nevertheless captured in the FSDS testbed. The magnitude of gravity gradient torque is a function of both spacecraft attitude and its distance from Titan. The gravity-gradient torque (Nm) about the spacecraft's [X, Y, Z] axes are given by:

$$\begin{aligned} T_{\text{GG}}^X(t) &= \frac{3\mu_{\text{Titan}}}{d(t)^3} (\bar{U}_R \bullet \bar{j})(\bar{U}_R \bullet \bar{k})(I_{YY} - I_{ZZ}) \\ T_{\text{GG}}^Y(t) &= \frac{3\mu_{\text{Titan}}}{d(t)^3} (\bar{U}_R \bullet \bar{i})(\bar{U}_R \bullet \bar{k})(I_{ZZ} - I_{XX}) \\ T_{\text{GG}}^Z(t) &= \frac{3\mu_{\text{Titan}}}{d(t)^3} (\bar{U}_R \bullet \bar{i})(\bar{U}_R \bullet \bar{j})(I_{XX} - I_{YY}) \end{aligned} \quad (3)$$

Here,  $\mu_{\text{Titan}}$  is the product of the universal gravitational constant and the mass of Titan ( $\approx 8.9782 \times 10^3 \text{ km}^3/\text{s}^2$ ). The set [i, j, k] represents unit vectors along the spacecraft's axes.  $U_R$  is the unit vector from Titan's center of mass to the spacecraft's center of mass, and  $d(t)$  (in km) is time-varying distance between the two centers of mass. The symbol " $\bullet$ " in equation (3) denotes the scalar product of two vectors. The moments of inertia (in  $\text{kg}\cdot\text{m}^2$ ) of the spacecraft about the [X, Y, Z] axes are denoted by  $I_{XX}$ ,  $I_{YY}$ , and  $I_{ZZ}$ , respectively. Representative value of gravity gradient torque is on the order of 0.001 Nm, about 1-2 order of magnitude smaller than the atmospheric torque.

Magnetic disturbance torque on the spacecraft results from the interaction between the spacecraft's residual magnetic field and the magnetic field of Saturn. With a worst-case spacecraft's attitude, the magnetic disturbance torque,  $T_{\text{Magnetic}}$ , could be estimated using the following expression:

$$T_{\text{Magnetic}} = M_{\text{arm}} \frac{B_{\text{Saturn}}}{r_{\text{ps}}^3} \quad (4)$$

Here,  $M_{\text{arm}}$  is the spacecraft magnetic moment arm, estimated to be 1.4 Amp- $\text{m}^2$ .  $B_{\text{Saturn}}$  is the magnetic flux density on the surface of Saturn, estimated to be about  $8.3\text{e-}5$  Tesla ( $\text{kg}\cdot\text{s}^{-2}\cdot\text{A}^{-1}$ ), and  $r_{\text{ps}}$  is the distance between Saturn and the spacecraft in planet radii. Near the Titan closest approach of a low-altitude Titan flyby,  $r_{\text{ps}}$  is about 20.3. Accordingly, the estimated worst-case magnitude of  $T_{\text{Magnetic}}$  is  $1.39\text{e-}8$  Nm. Like the gravity gradient torque, the magnetic disturbance torque is small when compared with the atmospheric torque. Other disturbance torque, due to direct solar radiation torque and the radiation torque due to the power generators are on the order of micro-Nm. These disturbances are not modeled in the FSDS testbed.

### 1. Modeling

In order to support Cassini's prime mission, a new capability was created to model Titan atmospheric torque. The model enables the verification of spacecraft's controllability during Titan low-altitude flyby encounters. There were twenty-one targeted low-altitude Titan science flybys before the end of the prime mission. Although there is confident that the on-board fault protection design will be able to recover the spacecraft from a tumbling scenario, it is undesired for the spacecraft to fly through the Titan atmosphere at altitudes with densities lower than these tumbling densities.

The Titan atmospheric torque model was originally modeled in a Kinematics Predictor Tool which supports ground software operations. The model was ported into FSDS and additional capabilities were implemented. To capture the project area and center of pressure of the spacecraft, fourteen angles were identified in the XZ plane. Additional effort was made to capture the silhouette of the Cassini spacecraft with and without the Huygens probe, main engine skirt, and with and without the main engine cover. This would provide a more accurate depiction of

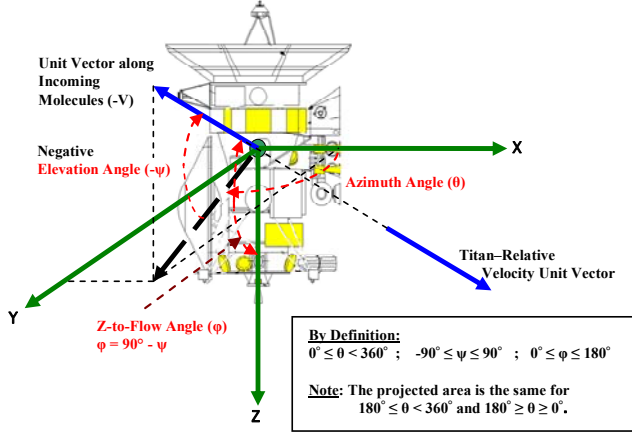


**Figure 5. Titan Model Angle Definitions.** Figure identifies angles for elevation angle, azimuth angle, and Z-to-flow. All needed as inputs to determine center of pressure and projected area needed to determine simulated atmospheric torque.

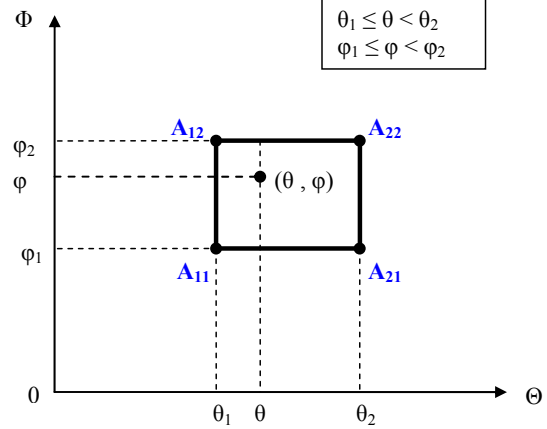


**Figure 6. Two-dimensional Linear Interpolation within a Grid. (From Reference 13)** Data is defined on the vertices of the grid. Given azimuth and elevation angle, correct center of pressure and projected area values are identified in a lookup table.

**Table 2. Nomenclature for the Projected Area and Center of Pressure (From Reference 13)**

Angle Pair	Projected Area (m <sup>2</sup> )	Center of Pressure Vector (m)
(θ <sub>1</sub> , φ <sub>1</sub> )	A <sub>11</sub>	CP <sub>11</sub>
(θ <sub>1</sub> , φ <sub>2</sub> )	A <sub>12</sub>	CP <sub>12</sub>
(θ <sub>2</sub> , φ <sub>1</sub> )	A <sub>21</sub>	CP <sub>21</sub>
(θ <sub>2</sub> , φ <sub>2</sub> )	A <sub>22</sub>	CP <sub>22</sub>
(θ, φ <sub>1</sub> )	A <sub>φ1</sub>	CP <sub>φ1</sub>
(θ, φ <sub>2</sub> )	A <sub>φ2</sub>	CP <sub>φ2</sub>
(θ, φ)	A <sub>θφ</sub>	CP <sub>θφ</sub>

spacecraft's projected area; however in only the XZ plane, which is a one-dimensional view (see Figure 5 as a reference). This was implemented in the form of a lookup table. This version of the model was released to support the first couple of low-altitude Titan flybys.

An update to the model was needed to provide more robust modeling capabilities to support multi-dimensional spacecraft orientations (two-dimensional views for projected area and center of pressure.) This version is currently the version used to support the remaining low-altitude Titan flybys. Since the spacecraft might be slewed during the flyby to achieve science objectives, the projected area will change continuously with time. The variation of the projected area with respect to the changing azimuth and elevation angles (between  $u_v$  and the spacecraft's body frame) is provided by model (see Figure 5 for azimuth and elevation angle definitions.) A convenient way to do this is to use a two-dimensional look-up table. Table 2 defines nomenclature for seven azimuth and elevation pairs used for interpolation. Figure 6 identifies the two-dimensional linear interpolation approach to identify the spacecraft projected area and center of pressure implemented in a tabular format.

To interpolate the projected area,<sup>13</sup>

For  $\varphi = \varphi_1 = \text{constant}$ ,

$$\frac{\theta - \theta_1}{\theta_2 - \theta_1} = \frac{A_{\varphi_1} - A_{11}}{A_{21} - A_{11}} \Rightarrow A_{\varphi_1} = A_{11} + \left( \frac{A_{21} - A_{11}}{\theta_2 - \theta_1} \right) (\theta - \theta_1) \quad (5)$$

For  $\varphi = \varphi_2 = \text{constant}$ ,

$$\frac{\theta - \theta_1}{\theta_2 - \theta_1} = \frac{A_{\varphi_2} - A_{12}}{A_{22} - A_{12}} \Rightarrow A_{\varphi_2} = A_{12} + \left( \frac{A_{22} - A_{12}}{\theta_2 - \theta_1} \right) (\theta - \theta_1) \quad (6)$$

Now, for  $\theta = \text{constant}$ ,

$$\frac{\varphi - \varphi_1}{\varphi_2 - \varphi_1} = \frac{A_{\theta\varphi} - A_{\varphi_1}}{A_{\varphi_2} - A_{\varphi_1}} \Rightarrow A_{\theta\varphi} = A_{\varphi_1} + \left( \frac{A_{\varphi_2} - A_{\varphi_1}}{\varphi_2 - \varphi_1} \right) (\varphi - \varphi_1) \quad (7)$$

Combine equations (5), (6), and (7) yield the interpolated projected area:

$$A_{\theta\varphi} = A_{11} + (A_{21} - A_{11}) \left( \frac{\theta - \theta_1}{\theta_2 - \theta_1} \right) + \left( \frac{\varphi - \varphi_1}{\varphi_2 - \varphi_1} \right) \left[ (A_{12} - A_{11}) + \left( \frac{\theta - \theta_1}{\theta_2 - \theta_1} \right) (A_{22} - A_{12} - A_{21} + A_{11}) \right] \quad (8)$$

Similarly for the interpolated center of pressure:

$$CP_{\theta\varphi} = CP_{11} + (CP_{21} - CP_{11}) \left( \frac{\theta - \theta_1}{\theta_2 - \theta_1} \right) + \left( \frac{\varphi - \varphi_1}{\varphi_2 - \varphi_1} \right) \left[ (CP_{12} - CP_{11}) + \left( \frac{\theta - \theta_1}{\theta_2 - \theta_1} \right) (CP_{22} - CP_{12} - CP_{21} + CP_{11}) \right] \quad (9)$$

To compute  $\theta$ ,  $\psi$ , and  $\varphi$  for a given  $-\hat{V} = f$  ( $f$  is the unit vector along drag force and  $V$  is the unit vector along the ram velocity of the spacecraft)

$$-\hat{V} = \hat{f} = \begin{bmatrix} f_x & f_y & f_z \end{bmatrix}^T$$

$$\theta = \left( \frac{180}{\pi} \right) \tan^{-1} \left( \frac{f_y}{f_x} \right) \quad (10)$$

If  $\theta < 0$ , then  $\theta = 360^\circ + \theta$

$$\varphi = \left( \frac{180}{\pi} \right) \cos^{-1}(f_z)$$

$$\Psi = 90^\circ + \varphi$$

The results of equations (8) and (9) are used in equation (1) to calculate the atmospheric torque which is applied as external stimuli on the FSDS DARTS model.

A key implementation of the model was to make all coefficients, parameters, and variables associated with Adler's approximation to Yelle's Titan density model modifiable. This would allow for tweaks and minor model updates without having to release a new version of FSDS. This also provided the flexibility to change the model's attributes to match closer to actual performance when validating simulation results with actual in-flight data.

This model has proven to be indispensable in helping the Cassini project to determine the safe altitude for each of the twenty-one low-altitude Titan flybys by simulating these flybys to determine the tumbling density. Along with this, the capability to generate gravity gradient torque to support RWA-controlled Titan flybys was also added to the model. This will enable the verification of RWA controllability during RWA-based Titan fly-bys.

## B. Titan Atmospheric Density Model Validation

The process of calibrating the Titan atmosphere density model implemented in the FSDS is illustrated below. After a Titan flyby (e.g., the first 950-km Titan-16 flyby in 2006), the atmosphere density (as a function of flyby altitude) is first estimated using the methodologies described in References 4 and 13. The peak torque imparted on the spacecraft usually occurs at the closest approach and the safety of the spacecraft for the flyby depends on it. As such, the "n" value in Equation (2) that produces a density estimate that best matches the telemetry data at the lowest

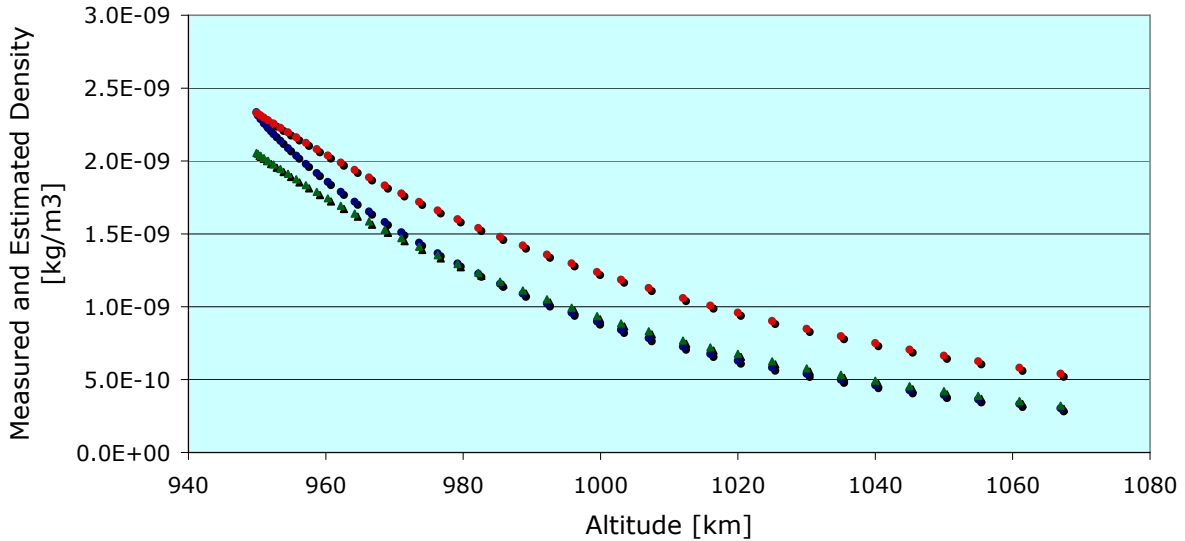


**Figure 7. Comparison of Titan Atmosphere Density.** *FSDS (Red and Green) versus Measured (Blue).*  
*Red: FSDS data using Equation (2)*  
*Green: FSDS data using Equation (11)*

flyby altitude is to be used by FSDS for that particular flyby. Using data from the 950-km Titan-16 flyby, the value of “n” determined is 1.435. A comparison between the density estimated using the flight data and that determined using Equation (2) (with n=1.435) is depicted in Figure 7. Note that, in general, the FSDS-based density is larger than its counterpart that is estimated using telemetry data. But the comparison is better near the Titan closest approach where the altitude is  $950 \pm 20$  km.

Using the methodologies described in Reference 4 and 13, the variations of Titan atmospheric density with altitude for a large number of low-altitude Titan flybys were reconstructed. The dependency of Titan atmospheric density with altitude for all reconstructed data could be represented by a single expression. But instead of using Equation (2), a simpler one-term expression was reported in Reference 13 via the least-square methodology:

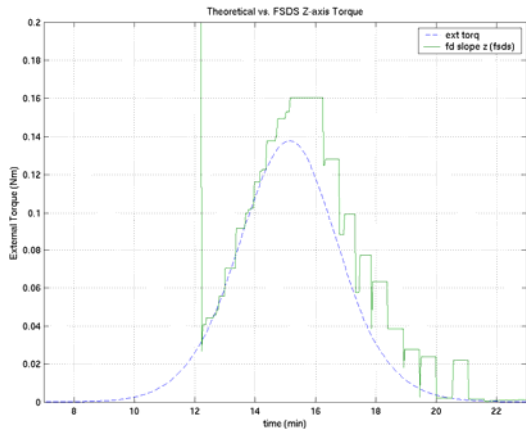


**Figure 8. Titan flyby FSDS prediction (From Reference 2).** *FSDS prediction of FSW telemetry measuring the Z-axis external torque caused by the density of Titan’s atmosphere at Titan-A, the first close Titan flyby at 1174 km.*

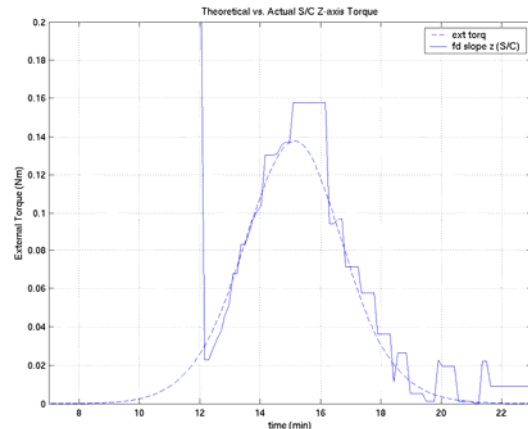


**Figure 9. Titan flyby in-flight S/C results (From Reference 2).** *FSW telemetry data measuring the Z-axis external torque caused by the density of Titan’s atmosphere at Titan-A, the first close Titan flyby at 1174 km.*

$$\rho_{\text{Titan}}(z) = 20.528 \times 10^{-10} \exp\left[-\frac{z-950}{63.11}\right] \quad (11)$$

The variation of Titan atmospheric density with altitude according to this expression is also given in Figure 7. Note that, density predicted using Equation (2) fit the measured data very well for altitudes higher than 970 km. Density predictions for altitudes lower than 970 km is poorer. This is one reason why the simpler expression shown in equation (11) wasn't implemented in FSDS.

The FSDS simulation results of external torque generated by a Titan flyby are given in Figure 8. To reconstruct Titan atmospheric density using in-flight data as shown in Figure 9, the use of several telemetry channels were exercised. The FSW has three high water mark channels that monitor thruster leak detection about the S/C X, Y, and Z axes.<sup>25</sup> Three minutes before Titan closest approach these channels were cleared. A minute after closest approach, the channels were cleared every 8 seconds to capture the digression of the actual torque profile caused by the atmosphere on the S/C. This methodology is described in Reference 24.

## VI. Enceladus Model Development and Validation

Recent Cassini observations of Enceladus, a small icy satellite of Saturn (with a mean radius of 247 km), confirmed the existence of a water vapor plume in the South polar region of Enceladus.<sup>14-21</sup> The Cassini's INMS detected atmospheric plume and coma out to a distance of >4,000 km from the surface of Enceladus.<sup>17</sup> Additionally, the radial and angular distributions of the INMS-based gas density estimates suggest a significant contribution to the plume from a source centered near the South polar cap of Enceladus. Reference 18 conjectured that the Enceladus plume might be the dominant source of materials in the Saturn's E ring system.

Measurements reported in References 14 and 20 revealed four prominent linear fractures, each separated by about 30 km and spanning 130 km in length straddling the southern polar region. These fractures, informally termed "tiger stripes," show dark flanks in the near-IR, and are identified individually as Alexandria, Cairo, Baghdad, and Damascus. The Tiger stripes are a likely source of tectonic activities and plume generation. From these Tiger stripes, materials are vented from the interior of the moon to hundreds of kilometers above the moon's surface. One estimate of the "height" of these plumes is 300 km from the surface.<sup>15</sup> Locations of the "tiger stripes" are depicted graphically in Figure 10 and tabulated in Table 3. Causes that led to the formations of these stripes are conjectured in Reference 21.

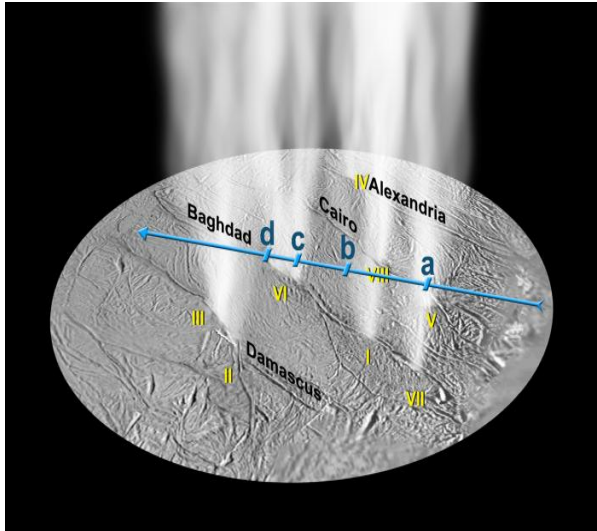


**Figure 10. Plume cone locations on Enceladus' southern pole (From Reference 20). Cone locations are described in Table 3.**

**Table 3. Latitudes and Longitudes of Tiger Stripes (From Reference 20)**

Cone	Tiger Stripe	Latitude(°)	Longitude (°W)
I	Baghdad	-81.5	32.8
II	Damascus	-79.4	315.5
III	Damascus	-81.3	292.8
IV	Alexandria	-72.9	148.7
V	Cairo	-78.6	72.3
VI	Baghdad	-87.1	231.4
VII	Baghdad	-74.6	29.8
VIII	Cairo	-82.1	115.5

## A. Enceladus Plume Density Model

In order to support the need to perform simulation testing for Enceladus flybys, an Enceladus plume density model was implemented in FSDS. The model was based on work reported in Reference 22. The objective of modeling the Enceladus plume density in FSDS is to allow AACS engineers to have the ability to simulate, as realistically as possible, the external torque imparted on Cassini spacecraft due to the jets and plumes during a low-altitude Enceladus flyby.

Prior to the implementation of this model, a tedious work-around of hand-editing scripts exists to apply a torque to the spacecraft given to that a torque profile is already known and available for each of the Enceladus flybys. However, this is not easily achievable if the S/C attitude is changing with time. This model provides the ability to change both attitude and altitude of a flyby. This capability increases the ability to simulate a multitude of fault testing scenarios which hand-edited scripts do not. The model gives AACS engineers the ability to test and exercise a gambit of scenarios in order to evaluate the spacecraft's AACS controllability and the plume's effect on the RWA spin rate during Enceladus flybys.

### 1. Modeling

The design of the plume model had to address and implement several key concepts which were different than the Titan atmospheric density model.

- 1) The geometry of the plume shall be modeled as eight truncated right circular cones
- 2) The location of the eight cones shall be defined as latitude/longitude pairs, which have been provided by the scientists (see Figure 10 and Table 3)
- 3) Each cone shall have a half-cone angle of  $45^\circ$  ( $\beta_m$ ) and shall be emanating from 1 km ( $w$ ) below the surface of Enceladus (see Figure 11)
- 4) All computations shall be done in the Enceladus-referenced coordinate frame
- 5) The model shall be active when the spacecraft is within the altitude of 8,000 km in respect to Enceladus
- 6) The two parameters,  $C$  and  $\epsilon$ , shall be the only parameters that are obtained by best fit of the E3 flight data
  - a. These parameters shall be adjusted as more flight data from future Enceladus flybys are captured and analyzed
- 7) For a typical flyby, based on the flyby latitude, longitude, and altitude, at every interval of time, the model shall check to see if the S/C is inside any of the eight truncated cones
  - a. When the spacecraft is inside a plume cone, the plume density shall vary as a function of altitude
  - b. Given a specific requirement, if the spacecraft is within the cylindrical jet inside the plume cone, the density of the plume jet shall be computed
- 8) The densities associated with the affecting cones shall be added together while taking into consideration the overlapping effect of the plume cones

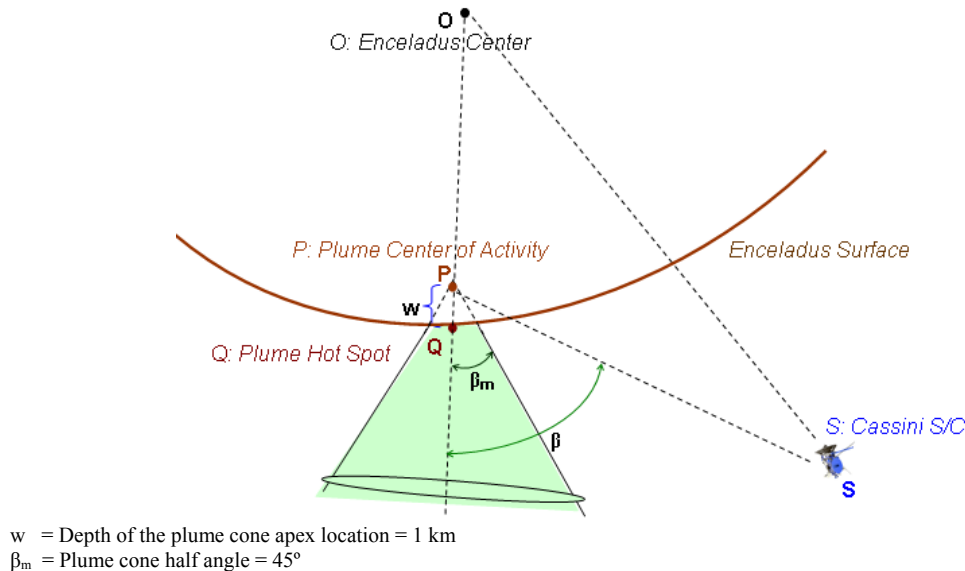
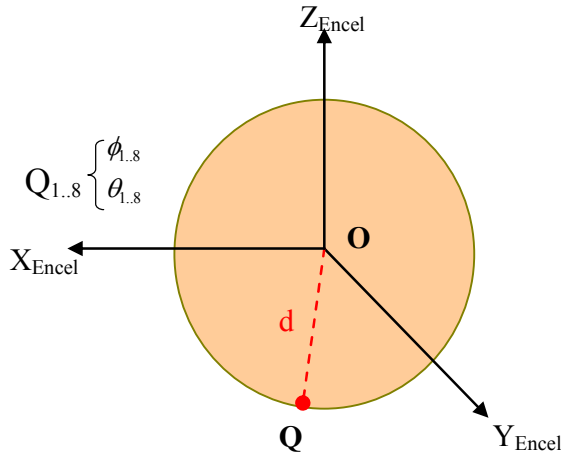


**Figure 11.** Model design of one of the Tiger Stripes. Graphical illustration of a single plume caused by a Tiger Stripe.



Where:  
**Q** is the hot spot on the surface of

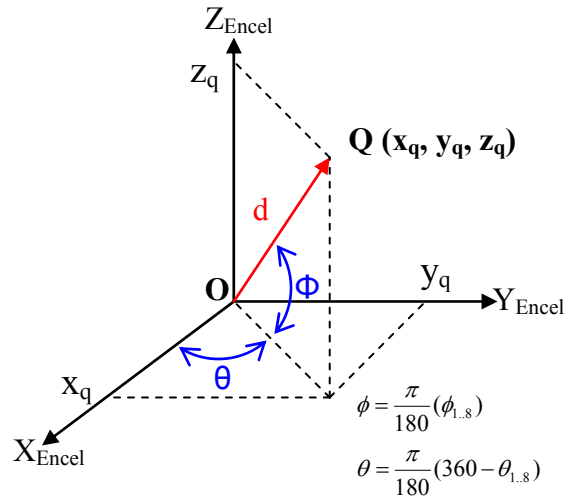


**Figure 12. Plume cone locations on Enceladus' southern pole.** Cone locations are described in Table 3.

**Figure 13. Coordinate Transformation**

Using the parametric equations of an ellipsoid to derive the position vector of the plume cone, solve for the distance,  $d$ , the distance between the apex of the plume cone and the center of Enceladus. Result is given in Equation (12)

$$\begin{aligned} \frac{x_q^2}{a^2} + \frac{y_q^2}{b^2} + \frac{z_q^2}{c^2} &= 1 \\ x_q &= d \cos \phi \cos \theta \\ y_q &= d \cos \phi \sin \theta \\ z_q &= d \sin \phi \end{aligned} \tag{12}$$

$$d = \frac{1}{\sqrt{\left(\frac{\cos \phi \cos \theta}{a}\right)^2 + \left(\frac{\cos \phi \sin \theta}{b}\right)^2 + \left(\frac{\sin \phi}{c}\right)^2}}$$

Where:

- $a$  = X-component of Enceladus tri-axial radii (256.6) [km]
- $b$  = Y-component of Enceladus tri-axial radii (251.4) [km]
- $c$  = Z-component of Enceladus tri-axial radii (248.3) [km]
- $\theta$  = Longitudinal location of the corresponding Enceladus plume cone [radian]
- $\phi$  = Latitudinal location of the corresponding Enceladus plume cone [radian]
- $x_q$  = X-axis location of the Enceladus hot spot in respect to Enceladus [km]
- $y_q$  = Y-axis location of the Enceladus hot spot in respect to Enceladus [km]
- $z_q$  = Z-axis location of the Enceladus hot spot in respect to Enceladus [km]

To derive the location of the hot spot on the surface (as shown in Figures 12 and 13) on Enceladus with respect to the center of Enceladus: ( $\hat{i}$ ,  $\hat{j}$ , and  $\hat{k}$  are unit vectors of the Enceladus coordinate frame)

$$\overrightarrow{OQ} = d * [(\cos \phi \cos \theta)\hat{i} + (\cos \phi \sin \theta)\hat{j} + (\sin \phi)\hat{k}] \tag{13}$$

To derive the location of the plume's center of activities (as shown in Figure 11) with respect to the center of Enceladus:

$$\overrightarrow{OP} = (d - w)[(\cos \phi \cos \theta)\hat{i} + (\cos \phi \sin \theta)\hat{j} + (\sin \phi)\hat{k}] \quad (14)$$

To derive the location of the spacecraft (as shown in Figure 11) with respect to the plume's center of activities:

$$\overrightarrow{PS} = \overrightarrow{OS} - \overrightarrow{OP} = \overrightarrow{OS} - (d - w)[(\cos \phi \cos \theta)\hat{i} + (\cos \phi \sin \theta)\hat{j} + (\sin \phi)\hat{k}] \quad (15)$$

To derive the unit vector for each of the following corresponding components:

$$\hat{U}_{OQ} = \frac{\overrightarrow{OQ}}{|\overrightarrow{OQ}|} \quad \hat{U}_{OP} = \frac{\overrightarrow{OP}}{|\overrightarrow{OP}|} \quad \hat{U}_{PS} = \frac{\overrightarrow{PS}}{|\overrightarrow{PS}|} \quad (16)$$

To derive the half-angle cone between the spacecraft and the each of the eight hot spots (as shown in Figure 11):

$$\beta = \frac{180}{\pi} \cos^{-1}(\hat{U}_{PS} \bullet \hat{U}_{OQ}) \quad (17)$$

Where:

- $OQ$  = Position vector of the plume hot spot with the respect to the center of Enceladus [km]
- $OP$  = Position vector of the plume center of activity with respect to the center of Enceladus [km]
- $OS$  = Position vector of the spacecraft with respect to the center of Enceladus [km]
- $PS$  = Position vector of the spacecraft with respect to plume center of activity [km]
- $\hat{U}_{OQ}$  = Unit vector of the center of Enceladus to the plume hot spot location [unitless]
- $\hat{U}_{OP}$  = Unit vector of the center of Enceladus to plume center of activity [unitless]
- $\hat{U}_{PS}$  = Unit vector of the plume center of activity to the spacecraft [unitless]
- $\beta$  = Computed half-angle between the S/C and the plume hot spot location with respect to the plume center of activity to determine whether the S/C is inside the plume cone[degrees]

To derive the angle between the spacecraft and plume hot spot with the respect to the center of Enceladus:

$$\beta_{SC-to-Jet} = \frac{180}{\pi} \cos^{-1}(\hat{U}_{OS} \bullet \hat{U}_{OQ}) \quad (18)$$

Where:

$$\hat{U}_{OS} = \text{Unit vector of the center of Enceladus to the spacecraft [unitless]}$$

To derive the minimum plume jet angle:

$$\beta_{Jet} = \sin^{-1}\left[\frac{w * \tan\left(\frac{\pi}{180} * \beta_m\right)}{|\overrightarrow{OS}|}\right] \quad (19)$$

Where:

$$|\overrightarrow{OS}| = \text{Magnitude of the spacecraft's position vector with the respect to the center of Enceladus [km]}$$

To derive the Enceladus plume density (see Reference 22) when the S/C is either inside the plume or inside the jet:

$$Density(t) = \frac{C}{(Z + Z_0)^{2-\epsilon}} \quad [\text{kg/m}^3] \quad (20)$$

Where:

- $C$  = Enceladus fit coefficient [ $\text{kg}/\text{m}^3 * \text{km}^{2-\epsilon}$ ]
- $Z$  = Spacecraft flyby altitude with respect to Enceladus (changing with time) [km]
- $Z_0$  = Fixed minimum Enceladus altitude (default value = 20) [km]
- $\epsilon$  = Enceladus fit exponential term (default value = 0) [unitless]

In order to effectively calibrate the effect of the Enceladus plume density when multiple cones are entered, the following equation (see Reference 22) was created to lessen the total density by a residual factor:

$$Density_{Effective}(t) = \sum_{i=1}^{\alpha_{Cone}} Density_i(t) - [ \epsilon_{Cone} * (\alpha_{Cone} - 1) * \sum_{i=1}^{\alpha_{Cone}} Density_i(t) ] \quad (21)$$

Where:  $\epsilon_{Cone}$  = A small residual value to offset the density when multiple plume cones are entered (default value = 0) [unitless]

$\alpha_{Cone}$  = Number of cones intercepted at time, t [unitless]

Rather than density varying with altitude like Titan, the Enceladus plume density varies with three variables: longitude, latitude, and altitude of the spacecraft. For a typical Enceladus flyby based on its flyby latitude, longitude, and altitude at every interval of time, the model checks to see if the S/C is inside the truncated cones. If so, the density is computed using the Enceladus density equation (Equation 20). In that expression, the first term, Z (in km), is the time-varying Enceladus-relative altitude of the spacecraft. The second term,  $Z_0$ , is the minimum fixed Enceladus altitude (20 km). The third term in this expression,  $\epsilon$  (unitless), represents the Enceladus fit exponential term. Lastly, the term, C, is the Enceladus fit coefficient ( $\text{kg}/\text{m}^3 * \text{km}^{2-\epsilon}$ ), which is equivalent to the “n” value in the Titan density model. A large “C” value will produce high density. This factor “C” is used to tune the Enceladus plume density model so that the resultant density matches flight results as close as possible.

**Table 4: Enceladus Model Default Parameter Table**

Parameter	A	B	Unit
C	3.911e-08	3.911e-08	$\text{kg}/\text{m}^3 * \text{km}^{2-\epsilon}$
$\epsilon$	0.0	0.0	unitless
w	1.0		km
$Z_0$	20	20	km
$\beta_m$	45	45	°

The second term,  $Z_0$ , is the minimum fixed Enceladus altitude (20 km). The third term in this expression,  $\epsilon$  (unitless), represents the Enceladus fit exponential term. Lastly, the term, C, is the Enceladus fit coefficient ( $\text{kg}/\text{m}^3 * \text{km}^{2-\epsilon}$ ), which is equivalent to the “n” value in the Titan density model. A large “C” value will produce high density. This factor “C” is used to tune the Enceladus plume density model so that the resultant density matches flight results as close as possible.

In order to account for the tidal frictional heating theory, two sets of the parameters (see Table 4) are created. Set “A” is used when the distance between Saturn and Enceladus is within a specified threshold distance ( $\sim 2.38036\text{E}+05$  km) at the time of Cassini spacecraft’s flyby encounter with Enceladus; otherwise, set “B” is used. The contents of these two sets of values are initially assumed to be identical but can be updated as more flyby data are collected. The distance between Enceladus and Saturn is computed during a FSDS flyby simulation. Depending on its range at the time of the flyby, one of the two sets is selected and used.

In modeling the limitations in the INMS detection capabilities, it was decided that the model shall only be active when the S/C is within 8000 km to Enceladus. Whether this is the case is still under conjecture, but it has no bearing to the model itself. Enceladus plume density is only applicable when S/C actually enters the plume. Given the hot spot location of the tiger strips, the half angle cone,  $\beta$ , is computed for all eight cones. At anytime, whenever  $\beta_i$  ( $i=1, \dots, 8$ ) is within  $45^\circ$  ( $\beta_m$ ), the Enceladus plume density model is active, and the plume density due to that particular plume cone is computed. If more than one cone is entered, the total density is the sum of the component density of the entered cones.

Other non-gravitational torque imparted on the spacecraft during a low-altitude Enceladus flyby includes gravity gradient torque. It is relatively small when compared with Enceladus plume torque but are nevertheless captured in the FSDS testbed. The magnitude of gravity gradient torque is a function of both spacecraft attitude and its distance from Enceladus. The gravity-gradient (GG) torque (Nm) about the spacecraft’s [X, Y, Z] axes are given by:

$$\begin{aligned}
E_{GG}^X(t) &= \frac{3\mu_{Encel}}{d(t)^3} (\bar{U}_R \bullet \bar{j})(\bar{U}_R \bullet \bar{k})(I_{YY} - I_{ZZ}) \\
E_{GG}^Y(t) &= \frac{3\mu_{Encel}}{d(t)^3} (\bar{U}_R \bullet \bar{i})(\bar{U}_R \bullet \bar{k})(I_{ZZ} - I_{XX}) \\
E_{GG}^Z(t) &= \frac{3\mu_{Encel}}{d(t)^3} (\bar{U}_R \bullet \bar{i})(\bar{U}_R \bullet \bar{j})(I_{XX} - I_{YY})
\end{aligned} \tag{22}$$

Here,  $\mu_{Encel}$  is the product of the universal gravitational constant and the mass of Enceladus ( $\approx 7.21108 \text{ km}^3/\text{s}^2$ ). The set  $[i, j, k]$  represents unit vectors along the spacecraft's axes.  $\bar{U}_R$  is the unit vector from Enceladus' center of mass to the spacecraft's center of mass, and  $d(t)$  (in km) is time-varying distance between the two centers of mass. The symbol " $\bullet$ " in equation (22) denotes the scalar product of two vectors. The moments of inertia (in  $\text{kg}\cdot\text{m}^2$ ) of the spacecraft about the  $[X, Y, Z]$  axes are denoted by  $I_{XX}$ ,  $I_{YY}$ , and  $I_{ZZ}$ , respectively. Representative value of gravity gradient torque is many orders of magnitude smaller than the torque exerted by the plume. Other disturbance torque, due to direct solar radiation torque and the radiation torque due to the power generators are on the order of micro-Nm. These disturbances are not modeled in the FSDS testbed.

## B. Enceladus Plume Density Model Validation

In order to validate the fidelity of the implementation of the Enceladus plume density, a methodology to use the in-flight data to derive the plume density was adopted. The two independent methods of using FSDS simulation data and in-flight telemetry data to determine the Enceladus plume density are vital in verifying the fidelity of the simulation model.

**Method 1** uses the per-axis Attitude Control Errors telemetry to reconstruct the magnitude of the disturbance torque imparted on the spacecraft. The attitude of the S/C was controlled by three RWAs during some of the Enceladus flybys (such as the 50-km Enceladus-3 on 12 March 2008 and the 50-km Enceladus-4 on 11 September 2008.) In the presence of a plume-induced disturbance torque, the 0.03-Hz (bandwidth) PD (Proportional + Derivative) RWA controller will experience small per-axis attitude control error. The "size" of these attitude control errors is related to the plume-induced disturbance torque. A disturbance torque is estimated and added to the S/C using the FSDS testbed (that has been configured to mimic the E3 or E4 flyby.) The disturbance torque is adjusted until the FSDS-based attitude control error (primarily the Z-axis) closely approximates its counterpart in the telemetry data (see Figure 14). The corresponding estimated plume density is depicted in Figure 16.

**Method 2** uses time rates of change of per-axis accumulated angular momenta telemetry to reconstruct the magnitude of the disturbance torque imparted on the spacecraft. In order to maintain the quiescent inertial attitude of the S/C, the three RWAs must "absorb" the angular momenta imparted on the S/C due to the (time-varying)

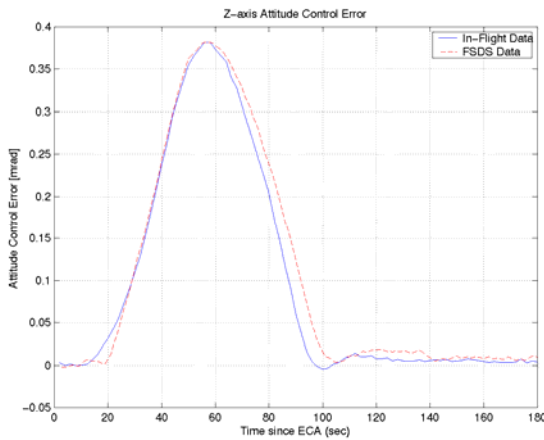


**Figure 14. Fitting Z-axis Attitude Control Error using Method 1.** Using FSDS, a good match between the FSDS-generated Z-axis attitude control error and flight data is achieved when the peak density is  $7.29\text{e-}12 \text{ kg/m}^3$ .

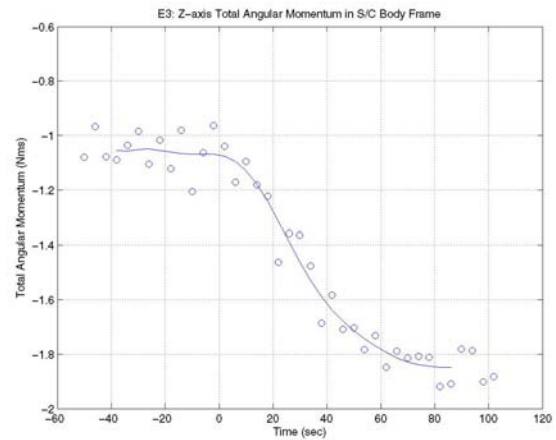


**Figure 15. Determining the Slope of Z-axis Total Angular Momentum using Method 2.** Using the Z-axis total angular momentum from the flight data to determine the peak slope, this is translated into a peak density of  $5.04\text{e-}12 \text{ kg/m}^3$ .

plume-induced torque. As a result, the RWAs' spin rates changed while the spacecraft is inside the plume. The per-axis accumulated angular momenta could be computed using knowledge of the RWA and S/C inertia properties, as well as telemetry data of the S/C's rates and RWA spin rates. The time rates of change of the three per-axis angular momenta are the (time-varying) per-axis torque imparted on the S/C. Plume density could be estimated using these three estimated torque. For E3, only the (relatively large) Z-axis torque is used to estimate the density because most of the imparted torque is about the Z-axis (see Figure 15).

The principle of conservation of angular momentum could be used to estimate the accuracy of the estimated plume density. If the density estimate is right, then the estimated plume-induced RWA spin rate perturbations (from entry to exit of the Enceladus plume) are given by Equation 23. Comparisons between these predicted RWA spin rate changes and those found via telemetry given in Table 5 indicates good comparison.

$$\begin{bmatrix} \Delta\Omega_1 \\ \Delta\Omega_2 \\ \Delta\Omega_4 \end{bmatrix} = \frac{30/\pi}{0.16} \begin{bmatrix} 0 & \frac{\sqrt{2}}{\sqrt{3}} & \frac{1}{\sqrt{3}} \\ -\frac{1}{\sqrt{2}} & -\frac{1}{\sqrt{6}} & \frac{1}{\sqrt{3}} \\ \frac{1}{\sqrt{2}} & -\frac{1}{\sqrt{6}} & \frac{1}{\sqrt{3}} \end{bmatrix} \begin{bmatrix} H_{Plume}^x \\ H_{Plume}^y \\ H_{Plume}^z \end{bmatrix} \approx \frac{30/\pi}{0.16} \begin{bmatrix} 0 & \frac{\sqrt{2}}{\sqrt{3}} & \frac{1}{\sqrt{3}} \\ -\frac{1}{\sqrt{2}} & -\frac{1}{\sqrt{6}} & \frac{1}{\sqrt{3}} \\ \frac{1}{\sqrt{2}} & -\frac{1}{\sqrt{6}} & \frac{1}{\sqrt{3}} \end{bmatrix} \begin{bmatrix} +9.9282E-03 \\ -4.2905E-01 \\ -9.1847E-01 \end{bmatrix} = \begin{bmatrix} -52.56 \\ -21.61 \\ -20.78 \end{bmatrix} \text{ rpm} \quad (23)$$

**Table 5. RWA Spin Rate Changes across the Enceladus Plume Cloud**

RWA	Predicted $\Delta\Omega$ (rpm) based on an assumed density	Flight $\Delta\Omega$ Data (rpm)	Error Magnitude of $\Delta\Omega$ (rpm)
RWA-1	-52.56	-47	-5.56
RWA-2	-21.61	-17	-4.61
RWA-4	-20.78	-20	-0.78
		Per-wheel mean error	3.65

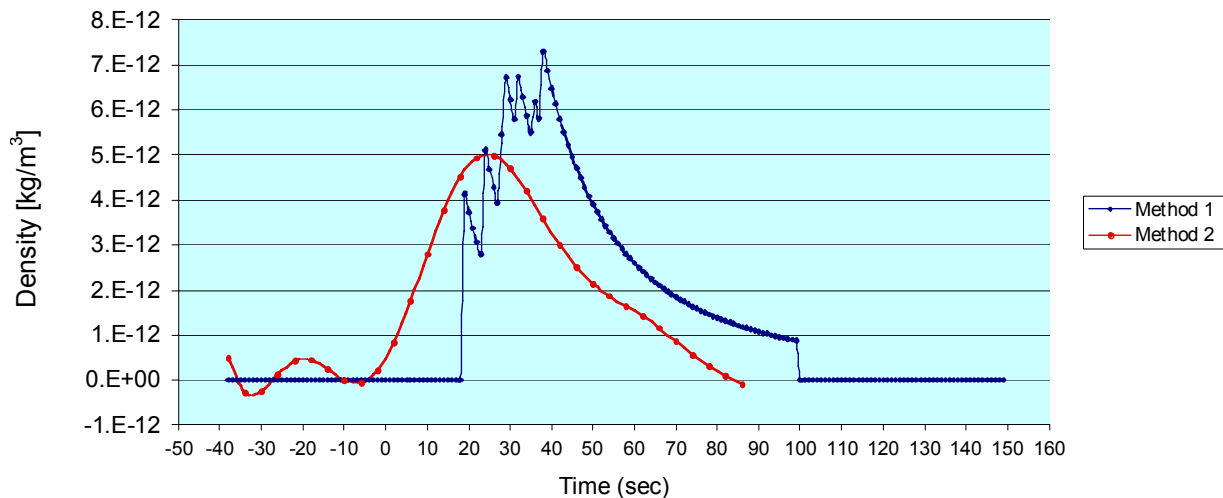


**Figure 16. E3 Plume Density Comparison.** Method 1 yields an average plume density of 6.50E-12 kg/m<sup>3</sup>. Method 2 yields a peak plume density of 5.04E-12 kg/m<sup>3</sup>.

## VII. The Role of Hardware-In-The-Loop Testbeds in Mission Operations

The Cassini Project has a set of equipment that has hardware in the loop testing capability known as the Integrated Test Lab (ITL) that consists of hardware and software that replicates the main engineering subsystems on the Cassini spacecraft,<sup>23</sup> which are the Command and Data Subsystem and the Attitude and Articulation Control Subsystem. One of the many advantages of having a real CDS in ITL is gives the ITL the capability to run the actual flight command sequences that will be used in flight, while having actual AACS hardware gives a high fidelity simulation of the AACS behavior during a flight sequence. In addition, having both AACS and CDS hardware in ITL yields the highest fidelity configuration possible on the ground that tests the interaction between AACS and CDS during a flight sequence test.

From the beginning both the ITL and FSDS testbeds shared core dynamics and environmental software models including the DARTS and the ephemeris models that allow the simulation of the dynamics and ephemeral environment on the AACS. In the case of the ITL, the external forces and torques from the environment and the thrusters must stimulate the actual Accelerometer and the IRU in order to simulate rates, torques, and acceleration on the S/C, and the ephemeral environment simulation must stimulate the actual Sun Sensor and Stellar Reference unit to replicate the response of these sensors mainly to the Saturnian bodies and the Sun. The ITL simulates the flight response of the sensors by adjusting the sensor stimulus (sensitivity and bias) to correspond with the best estimate of the current scale factor response and bias of the flight sensors.

During Titan and Enceladus flybys, the Cassini project gained a better characterization of the Titan atmospheric and Enceladus plume drag on the S/C as it flew by these bodies using engineering sensors and science instruments. The Titan atmospheric drag and Enceladus plume drag models were developed by the Cassini project in order to better simulate the forces and torques that would be imparted on the S/C as a function of altitude, velocity, and orientation, and atmospheric (Titan) or plume (Enceladus) density properties. This common algorithmic model was implemented in ITL after first being implemented and tested in FSDS. The ITL model used existing ephemeris tools to gather S/C to body info and the resulting atmospheric (Titan) or plume (Enceladus) forces and torques were added to the external forces and torques in the baseline model to yield acceleration and rate data used to stimulate the accelerometer and IRU sensors. Comparisons were made both between FSDS and ITL and ITL and the S/C for validation.

The ITL has needed to modify its simulation of both the Saturnian environment and the AACS sensor response as our characterizations of these factors has changed throughout the mission. During Saturn tour, some model changes implemented in ITL were usually first simulated in FSDS. After softsim validation, these algorithms and/or parameter changes were then implemented in the ITL simulation. This process helped to streamline troubleshooting of the algorithms, minimized duplication of effort in ITL, and made for easier validation. This is especially true when the ITL simulation was enhanced to include the torque and drag effects during Enceladus and Titan flyby scenarios. Adding all these modifications to the ITL hardware in the loop testbed has improved on the already high fidelity of the ITL and helped to further minimize risk to the Cassini mission.

## VIII. Conclusions

Whether a mission is scheduled to have a prime mission ranging from a few months to tens of years, the benefits of having a software simulator to expose FSW and its affecting subsystems to known mission environments far outweighs the initial cost of implementation.<sup>2</sup> The benefits of software simulators will increase in importance during the life of a mission, but only if testbeds are well maintained. Maintenance not only means the upkeep of current mission-specific parameters, but the ability to accurately model future significant spacecraft events. The Cassini project has recognized this fact and has encouraged the implementation of new high-fidelity environmental models and/or modification of existing parametric models to support tour, prime mission and extended mission operations. The majority of the effort was to support key scientific events. This paper has focused on two key models. The Titan and Enceladus density models have made it possible for the operations team to evaluate key scenario attributes within its corresponding mission phases:

- 1) Provided the ability to evaluate of spacecraft tumble scenarios. The Titan model identified safe flyby altitudes for each of the planned low-altitude Titan flybys. This allowed the mission planners to design science sequences years in advance of the actual flybys.
- 2) Provided the means to analyze nominal and off-nominal flyby scenarios. With the capabilities of modifying model parameters and injecting specific faults, FSDS provided the capability to perform a large number of test scenarios to envelope the nominal operating ranges and the effects of possible fault scenarios. As a result, several flyby sequences were modified based on test evaluations.

- 3) Provided the capability to perform post in-flight data reconstruction. Based on the high fidelity of each model to predict atmospheric or plume densities, the FSDS models became a key tool in reconstructing densities based on in-flight data.
- 4) Results from FSDS and ITL have influenced future Cassini mission objectives. Based on the findings from test scenarios involving the modeling of key environments, Scientists and Navigators were provided highly reliable and respected FSDS and ITL data to define orbit trajectories for the end of the prime mission, and the designs of the extended and extended-extended missions. FSDS was a key factor in identifying and defining flyby altitudes of both Titan and Enceladus.

The dynamics accuracy as a result of matching in-flight parametric data to be mimicked and modeled in a simulation test environment was a key part in making FSDS a trusted high-fidelity testbed for the project. The parametric updates to physics models and development of new models in FSDS have helped the implementation of similar models in the ITL. By validating the functionality of the models in a softsim before implementing them in an actual hardware environment increases the probability of implementation success.

The importance of model simulations in a faster-than-real-time softsim and a hardware-in-the-loop testbed was evidenced in the continued success of the Cassini mission. From FSDS's initial inception as a FSW test tool to its multipurpose role during operations; the continual efforts to evolve it and to accurately simulate a spacecraft's subsystem designs and its surrounding environments have benefited all pre-launch and post-launch design, development, test, and operations teams.

### Acknowledgments

The work described in this paper was carried out by the Jet Propulsion Laboratory, California Institute of Technology, under contract with the National Aeronautics and Space Administration. Reference to any specific commercial product, process, or service by trade name, trademark, manufacturer, or otherwise, does not constitute or imply its endorsement by the United States Government or the Jet Propulsion Laboratory, California Institute of Technology.

The authors would like to acknowledge Siamak Sarani for his contributions as the Guidance and Control analyst who provided many of the calculations and inputs to the design of both Titan and Enceladus models, and David M. Myers who initially implemented the Titan model in the Kinematics Predictor Tool.

Copyright 2009 California Institute of Technology. Government sponsorship acknowledged.

### References

- <sup>1</sup>Brown, J.M., "Cassini Attitude Control Flight Software: From Development to In-flight Operation," *16<sup>th</sup> AIAA Guidance, Navigation and Control Conference and Exhibit*, Honolulu, HI, Aug. 18-22, 2008.
- <sup>2</sup>Brown, J.M., Lam, D.C., Chang, L., Burk, T.A., and Wette, M.R., "The Role of the Flight Software Development System Simulator throughout the Cassini Mission," *AIAA Guidance, Navigation, and Control Conference and Exhibit*, AIAA-2005-6389, San Francisco, CA, Aug. 15-18, 2005.
- <sup>3</sup>Draper, R.F., "The Mariner Mark II Program," *AIAA 26<sup>th</sup> Aerospace Sciences Meeting*, AIAA-88-0067, Reno, NV, Jan. 11-14, 1988.
- <sup>4</sup>Lee, A.Y., and Hanover, G., "Cassini Attitude Control System Flight Performance," *AIAA Guidance, Navigation, and Control Conference and Exhibit*, AIAA-2005-6269, San Francisco, CA, Aug. 15-18, 2005.
- <sup>5</sup>Jain, A. and Man, G., "Real-Time Simulation of the Cassini Spacecraft Using DARTS: Functional Capabilities and the Spatial Algebra Algorithm," *5<sup>th</sup> Annual Conference on Aerospace Computational Control*, Aug. 1992.
- <sup>6</sup>Wang, E.K., and Brown, J.M., "Cassini Test Methodology for Flight Software Verification during Operations," *15<sup>th</sup> AIAA Guidance, Navigation and Control Conference and Exhibit*, Hilton Head, SC, Aug. 20-23, 2007.
- <sup>7</sup>Chang, L., Brown, J.M., Barltrop, K.J., and Lee, A.Y., "Use of Guidance and Control Test Cases to Verify Spacecraft Attitude Control System Design," *AAS/AIAA Space Flight Mechanics Meeting*, AAS 02-122, AIAA, Washington, DC, Jan. 2002.
- <sup>8</sup>Yelle, R.V., Strobell, D.F., Lellouch, E., and Gautier, D., "Engineering Models for Titan Atmosphere," in *NASA Special Publication 1177 entitled "Huygens: Science, Payload, and Mission"*, (editor: A. Wilson), August 1997.
- <sup>9</sup>Cassini Reveals Titan (with 7 papers), *Science*, Volume 308, No. 5724, May 13, 2005, pp. 978-992.
- <sup>10</sup>Stalder, J.R. and Zurick, V.J., "Theoretical Aerodynamic Characteristics of Bodies in a Free-Molecular-Flow Field," *NACA Technical Note 2423*, July 1951.
- <sup>11</sup>Emmons, H.W. (editor), *Fundamental of Gas Dynamics*, Volume III, High Speed Aerodynamics and Jet Propulsion, Princeton University Press, Princeton, New Jersey, 1958.
- <sup>12</sup>Stalder, J.R., Goodwin, G., and Creager, M.O., "A Comparison Between Theory and Experiment for High Speed Free Molecular Flow," *National Advisory Committee for Aeronautics*, NACA Technical Note 2244, 1950.
- <sup>13</sup>Sarani, S., "A Novel Methodology for Reconstruction of Titan Atmospheric Density Using Cassini Guidance, Navigation, and Control Data," Paper AIAA 2007-6343, *Proceedings of the AIAA Guidance, Navigation, and Control Conference*, August 20-23, Hilton Head, South Carolina, 2007.

- <sup>14</sup>Porco, C.C., Helfenstein, P., Thomas, P.C., Ingersoll, A.P., Wisdom, J., West, R., Neukum, G., Denk, T., Wagner, R., Roatsch, T., Kieffer, S., Turtle, E., McEwen, A., Johnson, T.V., Rathbun, J., Veverka, J., Wilson, D., Perry, J., Spitale, J., Brahic, A., Burns, J.A., DelGenio, A.D., Dones, L., Murray, C.D., Squyres, S., "Cassini observes the active south pole of Enceladus," *Science* 311, 43-64 (2006).
- <sup>15</sup>Hedman, M.M., Nicholson, P.D., Showalter, M.R., Brown, R.H., Buratti, B.J., and Clark, R.N., "Spectral Observations of the Enceladus Plume with Cassini-VIMS," *The Astrophysical Journal*, 693:1749-1762, 2009 March 10.
- <sup>16</sup>Matson, D.L., Castillo, J.C., Lunine, J., and Johnson, T.V., "Enceladus' plume: Compositional evidence for a hot interior," *Icarus* 187 (2007) 567-573.
- <sup>17</sup>Waite, H.J., et al, "Cassini Ion and Neutral Mass Spectrometer: Enceladus Plume Composition and Structure," *Science* 311, 1419 (2006).
- <sup>18</sup>Hansen, C.C., Esposito, L., Stewart, I.F., Colwell, J., Hendrix, A., Pryor, W., Shemansky, D., and West, R., 2006, "Enceladus' Water Vapor Plume," *Science* 311, 1422.
- <sup>19</sup>Hansen, C.C., Esposito, L., Stewart, I.F., Meinke, B., Wallis, B., Colwell, J., Hendrix, A.R., Larsen, K., Pryor, W., and Tian, F., "Enceladus' Water Vapor Jets Inside the Plume of Gas leaving Enceladus," *Nature*, Volume 456, No. 27, 477-479, November 2008.
- <sup>20</sup>Spitale, J.N., and Porco, C.C., "Association of the jets of Enceladus with the warmest regions on its south-polar fractures," *Nature* 449, 695-697 (2007).
- <sup>21</sup>Smith-Konter, B., and Pappalardo, R.T., "Tidally driven stress accumulation and shear failure of Enceladus's tiger stripes," *Icarus* 198, 435-451 (2008).
- <sup>22</sup>Sarani, S., "The Enceladus plume density modeling for Cassini Attitude and Articulation Control Subsystem," *Proceedings of the AIAA Guidance, Navigation, and Control Conference*, August 10-13, Chicago, IL, 2009.
- <sup>23</sup>Badaruddin, K.S., Hernandez, J.C., and Brown, J.M., "The Importance of Hardware-In-The-Loop Testing to the Cassini Mission to Saturn," *IEEE Aerospace Conference*, Track 12.0503, Paper 1231, Big Sky, MT, Mar. 3-10, 2007.
- <sup>24</sup>Feldman, A.W., Brown, J.M., Wang, E.K., Peer, S.G., and Lee, A.Y., "Reconstruction of Titan Atmosphere Density using Cassini Attitude Control Flight Data," *17<sup>th</sup> AAS/AIAA Space Flight Mechanics Meeting*, AAS-07-187, Sedona, AZ, Jan. 28-Feb. 01, 2007.
- <sup>25</sup>Lee, A.Y., and Brown, J.M., "A Model-Based Thruster Leakage Monitor for the Cassini Spacecraft," *Proceedings of the American Control Conference*, Philadelphia, PA, June 1998, pp. 902-904.